ISSN 0965-545X, Polymer Science, Series A, 2017, Vol. 59, No. 4, pp. 554–565. © Pleiades Publishing, Ltd., 2017.

COMPOSITES

Optical and Dielectric Properties of PVP Based Composite Polymer Electrolyte Films[1]

S. K. Shahenoor Basha[a], G. Sunita Sundari[a], K. Vijay Kumar[b], and M. C. Rao[c,*]

[a] *Solid State Ionics Laboratory, Department of Physics, K. L. University, Guntur 522502, India*
[b] *Department of Physics, Dayananda Sagar Academy of Technology and Management, Udayapura, Bangalore 560082, India*
[c] *Department of Physics, Andhra Loyola College, Vijayawada 520008, India*
**e-mail: raomc72@gmail.com*

Received October 9, 2016;
Revised Manuscript Received February 11, 2017

Abstract—Solid polymer electrolyte films were prepared by adding Al_2O_3 particles to poly(vinylpyrrolidone)-$MgCl_2 \cdot 6H_2O$ salt using solution cast technique. Various analytical techniques have been applied to characterize the prepared polymer films such as XRD, SEM, UV–Vis spectroscopy and AC conductivity. The structural analysis of pure poly(vinylpyrrolidone) complexed with $MgCl_2 \cdot 6H_2O$ salt showed orthorhombic lattice structure indicating its semi-crystalline nature. SEM analysis reveals the heterogeneous phase of nanocomposite polymer electrolyte systems. The conductivity of Al_2O_3 doped poly(vinylpyrrolidone) based solid polymer electrolyte was found to be 1.22×10^{-6} S/cm at room temperature for 85 : 15 weight composition. Electrochemical cell has been fabricated with the configuration $Mg^+/(PVP + MgCl_2 \cdot 6H_2O + Al_2O_3)/(I_2 + C +$ electrolyte) and its discharge characteristics were studied for a constant load of 100 kΩ. Various cell parameters such as open-circuit voltage, short circuit current, energy density and power density were calculated for the prepared samples.

DOI: 10.1134/S0965545X17040095

INTRODUCTION

The development of polymer systems with high ionic conductivity is one of the main objectives in polymer research. This is because of their potential applications as electrolytes in solid state batteries, fuel cells, electrochemical display devices/smart windows, photo- electrochemical cells etc. [1–3], due to their high conductivity, high energy density, wide electrochemical stability and easy processability. Intrinsically conducting polymers have attracted the attention of researchers because of their numerous applications [4, 5]. In recent years tremendous effort has been made in the preparation of solid polymer electrolytes. The recent research trends in the field of rechargeable lithium batteries are directed towards the development of cells with high energy density (W h/kg) and high power density. A primary work in the field of solid polymer electrolyte has been carried-out by Wright et al. [6, 7] and found that the ionic conductivity is in the order of 10^{-5} S/cm at 330 K in PEO and NaSCN complexes.

A wide range of interest has been focused to prepare solid polymer electrolytes over a few decades due to their potential applications as electrolyte materials in high energy density batteries, rechargeable batteries and solid state batteries [8, 9]. The reason for growing interest in polymer nanocomposites (PNCs) is the recent availability of functional nanoparticles (NPs) that impart materials with unique electric, optical and magnetic properties [10, 11]. The results are thus attributed to interphase polymer with enhanced properties due to chemical and geometric confinement of polymer chains near the nanoparticle–polymer interfaces. In the design of nanocomposites and structures, the information about the intensity and thickness of interphase layer is essential, yet in many cases, such information is unavailable for the specific material systems [12–14]. The effects of dispersing insulating ceramic filler particles such as Al_2O_3, SiO_2 and TiO_2 on various physical/electrolytic properties of NCPEs have been investigated by various workers [15–17]. It has been observed, in general, that the particle size and the physical nature of the dispersed particles play a significant role. Hence, dispersal of nano-sized ceramic filler particles has been found to be more effective in

[1] The article is published in the original.

the NCPE systems, especially in terms of improvement in mechanical, physical and electrochemical properties. The enhancement in electrical conductivity due to the addition of inert filler particles has been generally explained in terms of the disruption of crystallization in the polymer host matrix.

Magnesium is used as the excellent material for anode in solid state batteries which is naturally available in earth crust. In addition magnesium based devices are much cheaper than lithium devices, whereas magnesium is less reactive, non-toxic than the lithium in ambient temperatures and atmospheric conditions. So magnesium is used instead of lithium for solid state battery application [18]. The order of conductivity of pure poly(vinylpyrrolidone) (PVP) is found to be in the range from 10^{-9} to 10^{-7} S/cm at room temperature and it is not suitable for battery applications. The order of ionic conductivity was improved from 10^{-7} to 10^{-5} S/cm by the addition of nanoparticles of Aluminum oxide (Al_2O_3) to magnesium chloride hexahydrate ($MgCl_2 \cdot 6H_2O$) salt. Gregory et al. [19] reported the electrochemical reversible deposition and dissolution process in $(Mg\ Bph_2Bu_2)_2$, where poly(vinylpyrrolidone) has played major role in displaying dissolubility, stability, high dielectric constant and compatibility. PVP is soluble in polar solvents as well as in ionized water. It is thermally stable and cross linked with the composites having high mechanical strength. PVP is chosen because it has good mechanical, electrical and optical characteristics. Pyrrolidone group of PVP prefers to incorporate with organic and inorganic salts resulting in the formation of film which has good dispersion and surface formation [20]. Solid polymer electrolyte complexed with inorganic salt and nano-fillers/plasticizers was first introduced by Weston and Steele in 1982 [21]. The addition of the fillers in the solid polymer electrolytes improves the electrical and mechanical strengths of the polymer [22].

It has been widely reported that adding small amounts of Al_2O_3 nanoparticles to polymers results dramatic changes in physical, mechanical, thermal properties and impart novel properties for biological, energy and sensing applications for host materials [23–25]. In particular, NPs have been widely used to modify and improve polymer properties by assembling them into nanostructures with a tunable length and morphology [26]. The purpose of this work is to improve the ionic conductivity of the prepared polymer electrolytes. In order to improve the mechanical integrity, SPEs are dispersed with micro- and nano-sized ceramic fillers of Al_2O_3 into the polymer salt matrix in the present paper. It has been shown that nano-sized ceramic filler particles incorporated into the polymer salt matrix can act as solid plasticizers inhibiting crystallization kinetics and promoting the retention of the amorphous phase down to sub-ambient temperatures. These nanocomposite polymer electrolytes have shown enhanced ionic conductivities with improved mechanical and thermal stability. They also have better electrochemical stability towards a metal anode and an enhanced cation transport number. In the present investigation, solid polymer electrolyte films were prepared by adding Al_2O_3 particles to PVP-$MgCl_2 \cdot 6H_2O$ salt to improve the ionic conductivity, which is suitable for battery application. These polymer electrolyte films were characterized by several experimental techniques. By using these solid polymer electrolytes, an electrochemical cell has been fabricated and discharge characteristics were studied for a constant load of 100 kΩ.

EXPERIMENTAL

Sample Preparation

Poly(vinylpyrrolidone) (PVP) was purchased from Sigma Aldrich chemicals Ltd., India with average molecular weight of 3.6×10^4. Aluminum oxide nanoparticles (99.9% purity) and magnesium chloride hexahydrate (99.5% purity) with melting point of 118°C were purchased from Loba chemicals Ltd., India and were used without further purification. PVP based solid polymer electrolyte films doped with magnesium chloride hexahydrate salt were prepared in different weight ratios (95 : 5, 90 : 10, 85 : 15, and 80 : 20) while dispersing Al_2O_3 nanoparticles in PVP : $MgCl_2 \cdot 6H_2O$: x wt % of Al_2O_3 (x = 1, 2, 3, and 4%) by using solution cast technique using double sterilized water as solvent. The mixture was stirred for 24 hours to obtain a homogeneous solution. Later the nanocomposite polymer solution was placed in the polypropylene dishes and placed in hot air oven at 60°C to remove the solvent trace in the polymer films. Later the films were taken off from the dishes and then placed in a desiccator until further test.

Characterization

X-ray diffraction pattern of the prepared sample was recorded on Bruker D8 instrument with CuK_α radiation. Morphological studies are performed on the prepared samples with different resolutions by using FE-SEM, Carl Zeiss, Ultra 55 model. Optical absorption studies were performed at room temperature using JASCO V-670 Spectrophotometer for the prepared samples in the wavelength region 200–800 nm. The Dielectric and impedance measurements of the prepared films were carried-out on HIOKI 3532-50 LCR Heister attached to a homemade sample holder having parallel plate circular electrodes. All measurements were carried-out in the range from 42 Hz to 1 MHz. Discharge characteristics were studied by fabricating a solid state battery with the configuration Mg

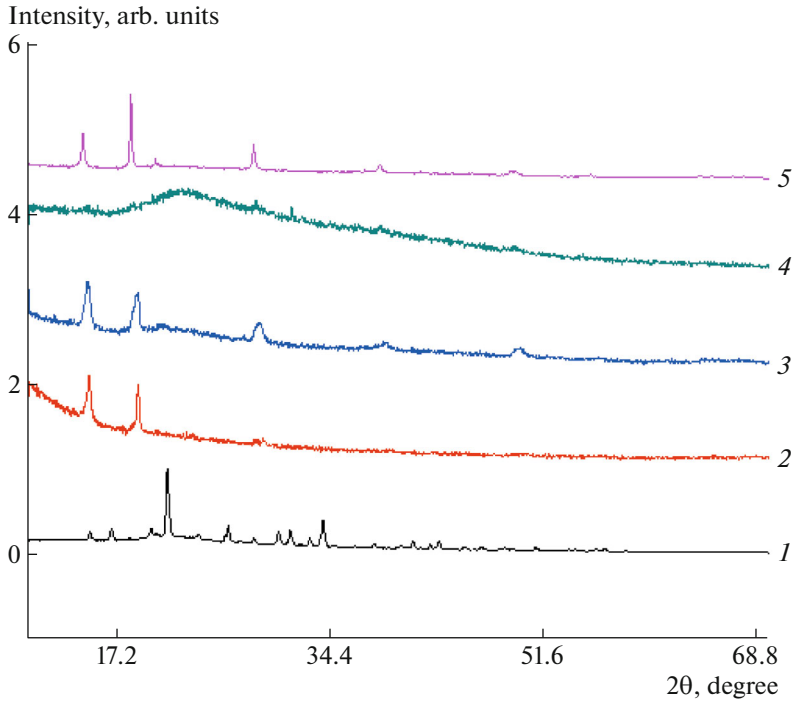

Fig. 1. (Color online) XRD analysis of polymer electrolyte films for different wt % ratios of PVP: (*1*) pure PVP, (*2*) (95 : 5), (*3*) (90 : 10), (*4*) (85 : 15), (*5*) (80 : 20).

(anode)/polymer electrolyte/(I + C + electrolyte)/(cathode) for various samples for a constant load of 100 kΩ at room temperature by Keithley electrometer 5641.

RESULTS AND DISCUSSION

XRD Studies

The structural analysis of pure PVP complexed with $MgCl_2 \cdot 6H_2O$ salt doped with nano-sized Al_2O_3 was shown in Fig. 1. Pure PVP shows a wide narrow peak lie in between 10–70° which corresponds to crystalline orthorhombic lattice indicating its semi-crystalline nature. By increasing the salt concentration to the polymer, small peaks with low intensities are observed; it evidently shows the presence of nanoparticles of Al_2O_3 in the host polymer [27]. It is clear from the Fig. 1 that the sharp peaks with small intensities are observed due to the semi-crystalline nature of the nanocomposite polymer films with 5, 10, and 20% weight ratios. But for 15% weight ratio no sharp peaks are observed due to the complete dissolution of the salt with the polymer which in turns the semi-crystalline to amorphous phase. Thus the polymer electrolyte is more flexible results in an increase in segmental motion of the polymer which enhances the ionic conductivity for 15% weight ratio of the polymer electrolyte [28].

As the salt concentration increases the intensity of the peaks also increases due to flexible back bone and crystalline nature which results in high ionic conductivity. As shown in Fig. 1, if the intensity of the peak decreases; this results that the salt percentage in the sample is completely mixed with the polymer suggesting a decrease in the degree of crystallinity of the complex. If no peaks are observed in the intensity region which indicates that there is a complete dissolution of the salt in the polymer matrix.

SEM Analysis

SEM image of different compositions of [PVP-$MgCl_2 \cdot 6H_2O$] : *x*% Al_2O_3 nanoparticles is shown in Fig 2. The images reveal the heterogeneous phase of nanocomposite polymer electrolyte systems. It is also observed that inorganic salt chunks are formed in polymer films which are completely dispersed in polymer film. The salt chunks are formed uniformly on the surfaces of the films with different degrees of roughness. SEM image shows the addition of nanoparticles disturbs the crystalline nature of the original matrix. The roughness of the film is also increased at higher concentration, which leads to ionic conductivity [29]. It is clear from the Fig. 2 that the small chunks present represent the phase separation between PVP and $MgCl_2 \cdot 6H_2O$: *x*% Al_2O_3 for 5, 10, and 20% weight ratios due to undissolved salt, which reveals that the salt concentration is incompletely incorporated in the

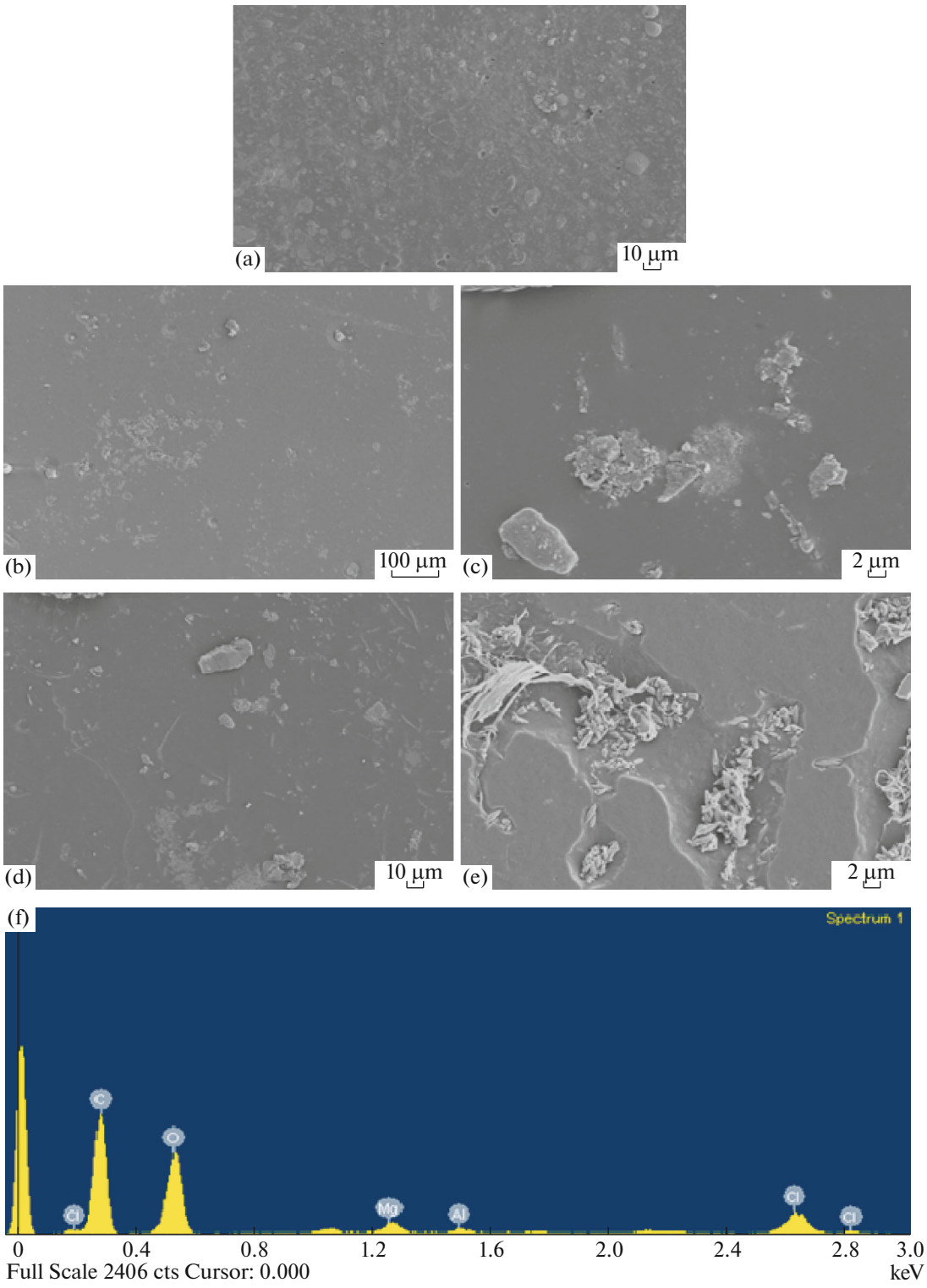

Fig. 2. (Color online) (a)–(e) SEM and (f) EDS analysis of polymer electrolyte films for different wt% ratios of PVP: (a) pure PVP, (b) (95 : 5), (c) (90 : 10), (d) (85 : 15), (e) (80 : 20).

host polymer. But for 15% weight ratio a complete dissolution takes place and no phase separation is observed in the host polymer which enhances the ionic conductivity. SEM result agrees with the XRD analysis. The element which is incorporated with the nanopolymer films was analyzed with the EDS system.

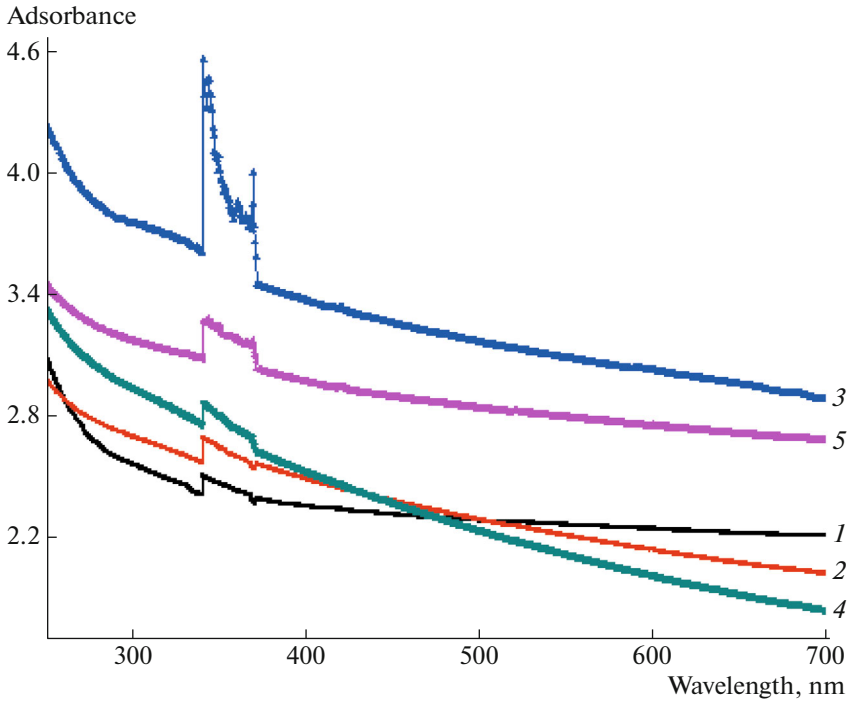

Fig. 3. (Color online) UV–Vis spectra of polymer electrolyte films for different wt% ratios of PVP: (*1*) pure PVP, (*2*) (95 : 5), (*3*) (90 : 10), (*4*) (85 : 15), (*5*) (80 : 20).

Optical Properties

UV–Vis spectroscopy is a versatile tool which is used for the identification of intra molecular vibrations or inorganic complexes in solution. UV–Vis spectra of pure PVP, PVP/$MgCl_2 \cdot 6H_2O/Al_2O_3$ nanoparticles with different ratios are shown in Fig. 3 in the wavelength range 300–700 nm. Due to the clusters between the vibrations of molecules a broad peak is obtained in the wavelength region 340–360 nm. Two spectral peaks are observed: one is at 350 nm which is due to the π–π* transition [30]. Another small peak is at 425 nm which is correlated with the benzene and quinone rings in the polymer chain [31].

Optical analysis is used to identify the optical band gap of the materials in the transmitting radiation. In an energy level a photon is absorbed, when an electron jumps from lower energy level to higher energy level. Transition takes place in bandgap energy as it rises in the absorption process called absorption edge from where the optical bandgap energies are determined.

Insulators and semiconductors are classified in to two types: direct bandgap and indirect bandgap. The top of the valence band and bottom of the conduction band are same, i.e., zero crystal momentum then direct bandgap takes place, where as in indirect bandgap if the top of the valence band and bottom of the conduction band are not same, i.e., non-zero crystal momentum. The indirect bandgap transitions takes place from valence band to conduction band which is accumulated with phonon of magnitude of crystal momentum [32]. The direct, indirect bandgaps and absorption edge values are shown in Table 1.

Table 1. Energy bandgap values for different compositions of polymer films

Polymer electrolyte	Optical bandgap		Absorption edge
	direct, eV	indirect, eV	
Pure PVP	3.99	3.67	4.25
PVP + $MgCl_2 \cdot 6H_2O + Al_2O_3$ (95 : 5)	3.50	3.46	3.69
PVP + $MgCl_2 \cdot 6H_2O + Al_2O_3$ (90 : 10)	3.48	3.31	3.61
PVP + $MgCl_2 \cdot 6H_2O + Al_2O_3$ (85 : 15)	3.28	3.15	3.42
PVP + $MgCl_2 \cdot 6H_2O + Al_2O_3$ (80 : 20)	3.32	3.29	3.50

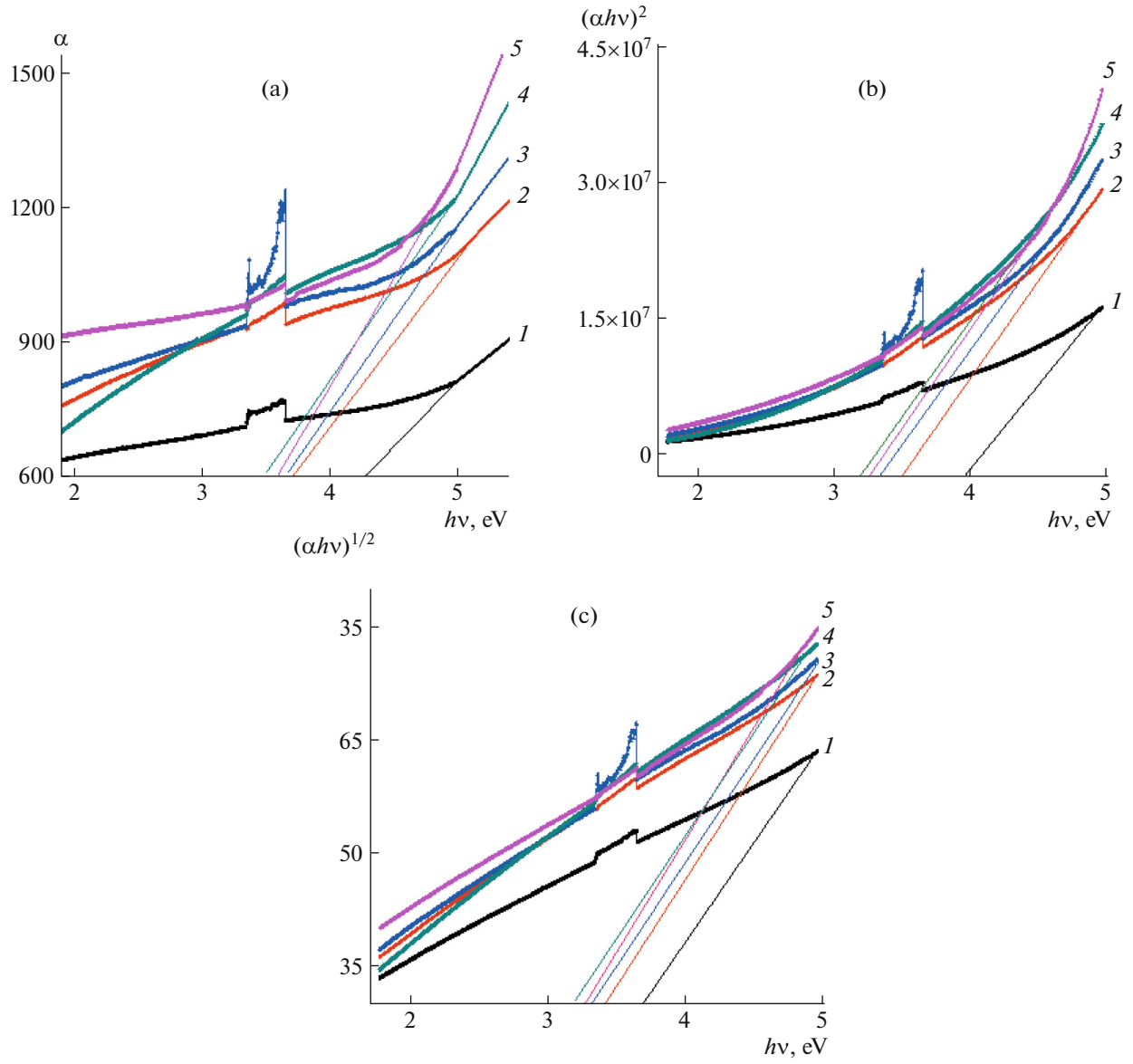

Fig. 4. (Color online) (a) α vs $h\nu$ plots, (b) α vs $(\alpha h\nu)^2$ plots and (c) α vs $(\alpha h\nu)^{1/2}$ plots of polymer electrolyte films for different wt % ratios of pure PVP and polymer electrolytes: (*1*) pure PVP, (*2*) (95 : 5), (*3*) (90 : 10), (*4*) (85 : 15), (*5*) (80 : 20).

To calculate bandgap energy values, graphs were plotted between absorption coefficient α, $(\alpha h\nu)^2$ and $(\alpha h\nu)^{1/2}$ as a function of $h\nu$. Absorption value for 5, 10, 15, and 20% weight ratios of $MgCl_2 \cdot 6H_2O$ salt doped with Al_2O_3 PVP films lies at 4.25, 3.69, 3.61, 3.42, and 3.50 eV, which is observed from Fig. 4. In the case of direct bandgap transitions, the absorption coefficient and energy of incident photon can be determined as follows [33–35]:

$$\alpha h\nu = C\,(h\nu - E_g)^{1/2}, \qquad (1)$$

where E_g is the band gap, C is a constant dependent on the specimen structure, α is the absorption coefficient, ν is the frequency of incident light and h is Planck constant. From the graph $(\alpha h\nu)^2$ versus $h\nu$, direct bandgap values are obtained. Energy gap values are 3.99, 3.50, 3.48, 3.28, and 3.32 eV as shown in Fig. 4b. Whereas indirect bandgap values are obtained by plotting $(\alpha h\nu)^{1/2}$ versus $h\nu$ as shown in Fig. 4c and the values obtained from the graph are 3.67, 3.46, 3.31, 3.15, and 3.29, respectively.

In the case of indirect transitions, phonon assistance is required for transition where the absorption coefficient has the following dependence on photon energy [33–35]:

$$\alpha h\nu = A(h\nu - E_g - E_p)^2 + B(h\nu - E_g - E_p)^2, \qquad (2)$$

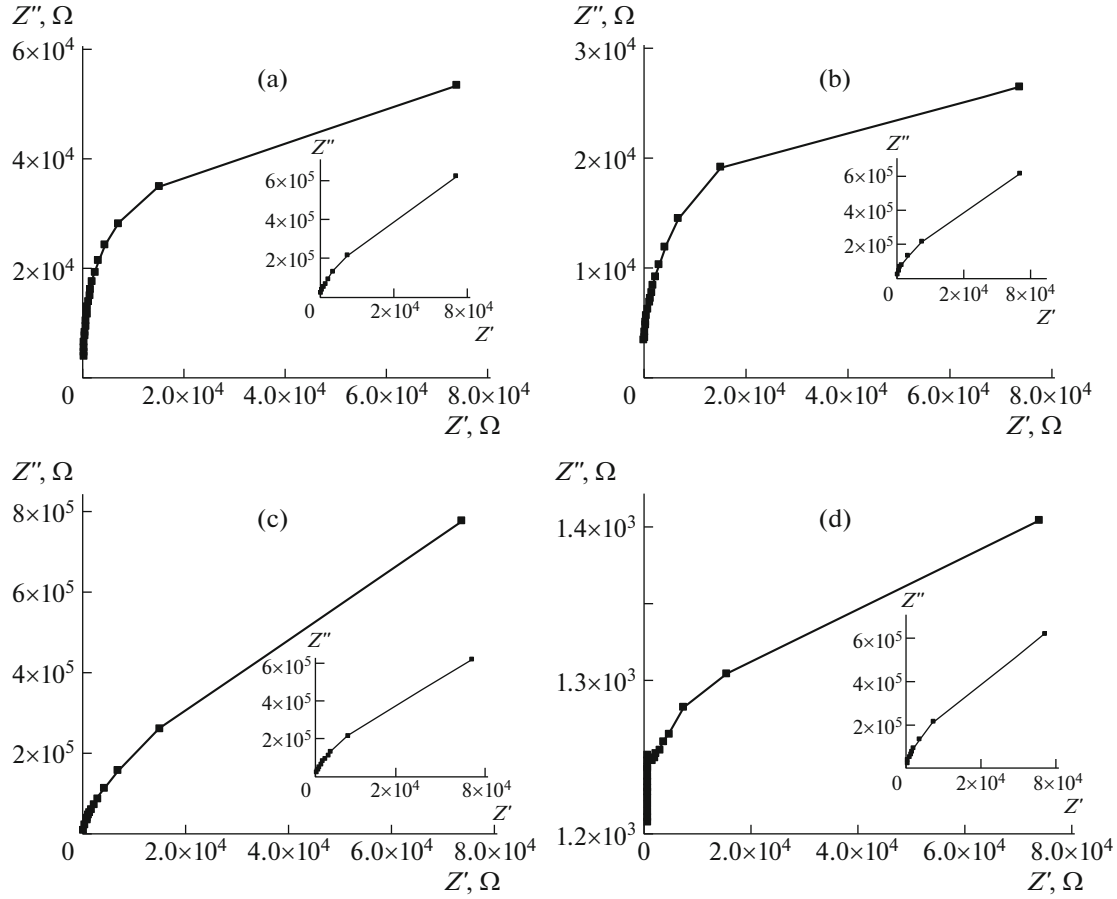

Fig. 5. Cole-Cole plots of polymer electrolyte films for different wt % ratios of PVP: (a) (95 : 5), (b) (90 : 10), (c) (85 : 15), (d) (80 : 20).

where E_p is the energy of the photon associated with the transition, A and B are constants depending on the band structure. From the obtained values it is clear that due to incorporation of small amount of dopant in a host lattice results in the decrease of activation energy in polymer chain such that the ionic conductivity is increased, which is observed from Fig. 4c. The direct and indirect bandgap values are shifted to lower energies on doping Al_2O_3 nanoparticles with increase of content of $MgCl_2 \cdot 6H_2O$ salt.

The polymer electrolytes were prepared by doping the salt with the polymer by incorporating nanoparticles of Al_2O_3 with different ratios of 5, 10, 15, and 20% [PVP-$MgCl_2 \cdot 6H_2O$] : x% Al_2O_3. From the optical properties one can reveal that for composition of 15% the bandgap energy is the lowest among all weight ratios. As a result the band edge, direct bandgap and indirect bandgap values showed a decrease with the increase of $MgCl_2 \cdot 6H_2O : x\%$ Al_2O_3 which is responsible for the defects in the polymer films. These defects produce the localized states in the optical bandgap [36]. In other words the decrease in the optical bandgap results in increase in the degree of disorder in the films. These results are in agreement with those obtained from A. C. conductivity in the present work.

A. C. Conductivity Studies

Figure 5 represents the Cole-Cole plots of the prepared solid polymer electrolyte samples for different weight ratios. Complex impedance plot shows a semicircular arc at high frequency region and a spike shows at the low frequency region. But in Fig. 5, a semicircular arc is not obtained and a spike is observed which results that the majority charge carriers flows in the solid polymer electrolyte is mostly due to ions. Due to the good contacts between electrode-electrolyte interfaces an electrode polarization phenomenon occurs. The Cole-Cole plot is obtained from the real part Z^{I} vs an imaginary part Z^{II} and the ionic conductivity calculated by using the relation:

$$\sigma_{ac} = t/(R_b x A), \quad (3)$$

where R_b is the bulk resistance, t is the thickness of the solid polymer electrolyte and A is the area of the elec-

Table 2. A. C. conductivity values for different compositions of polymer films

Films	Conductivity at RT, S/cm
Pure PVP	2.32×10^{-9}
PVP + $MgCl_2 \cdot 6H_2O$ + Al_2O_3 (95 : 5)	2.32×10^{-8}
PVP + $MgCl_2 \cdot 6H_2O$ + Al_2O_3 (90 : 10)	5.81×10^{-7}
PVP + $MgCl_2 \cdot 6H_2O$ + Al_2O_3 (85 : 15)	1.22×10^{-6}
PVP + $MgCl_2 \cdot 6H_2O$ + Al_2O_3 (80 : 20)	3.01×10^{-6}

trolyte. The calculated values of A. C. conductivity are shown in Table 2.

Dielectric Properties

The dielectric spectroscopy, impedance analysis studies were carried-out by using HIOKI 3532-50 LCR Heister in the frequency range from 42 Hz to 1 MHz at room temperature. The conductivity of the sample and the obtained data was analyzed. Figure 6a shows the variation of relative permittivity ε' along with the frequency and also concludes by increasing the frequency the relative permittivity ε' decreases sharply. Decrease in dielectric constant with increase in frequency is due to polar-

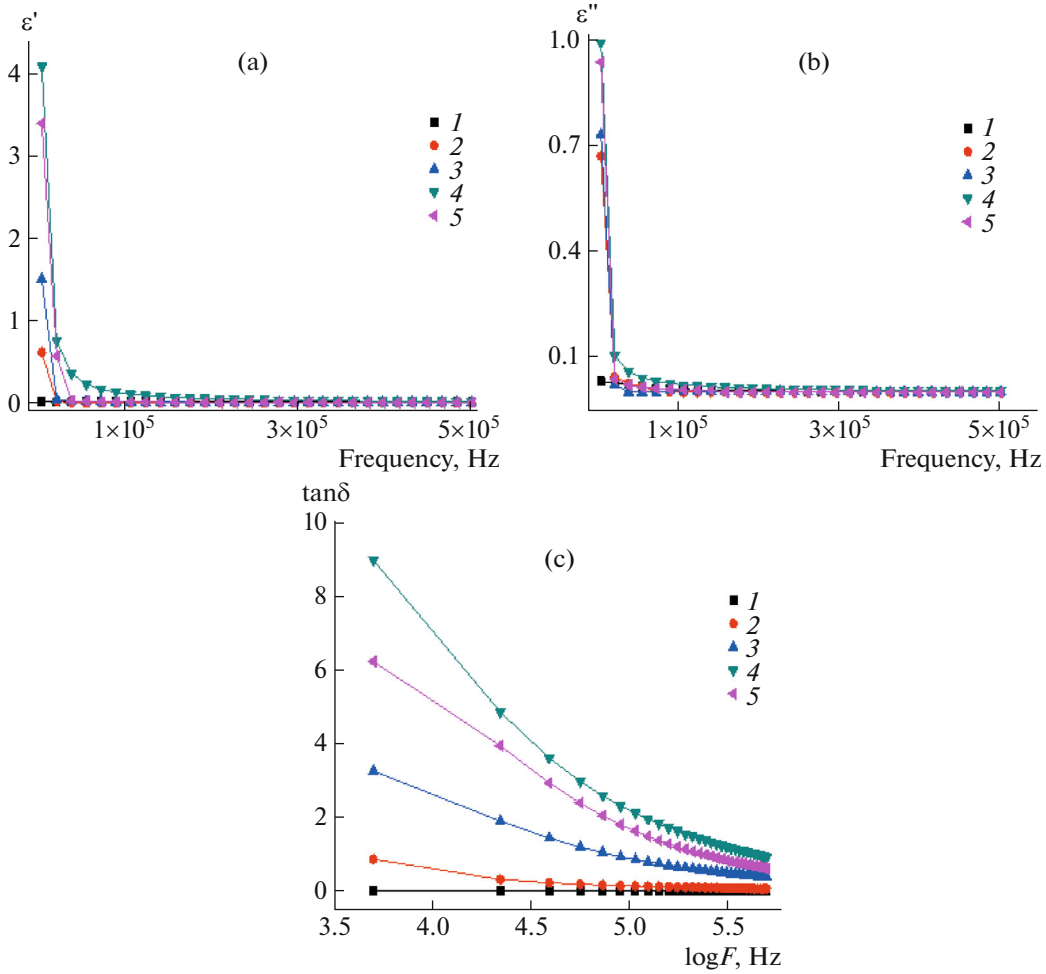

Fig. 6. (Color online) Variation of the real (a) and imaginary part (b) of dielectric constant and of the tangent loss (c) with frequency of polymer electrolyte films for different wt % ratios at 303 K: (*1*) pure PVP, (*2*) (95 : 5), (*3*) (90 : 10), (*4*) (85 : 15), (*5*) (80 : 20).

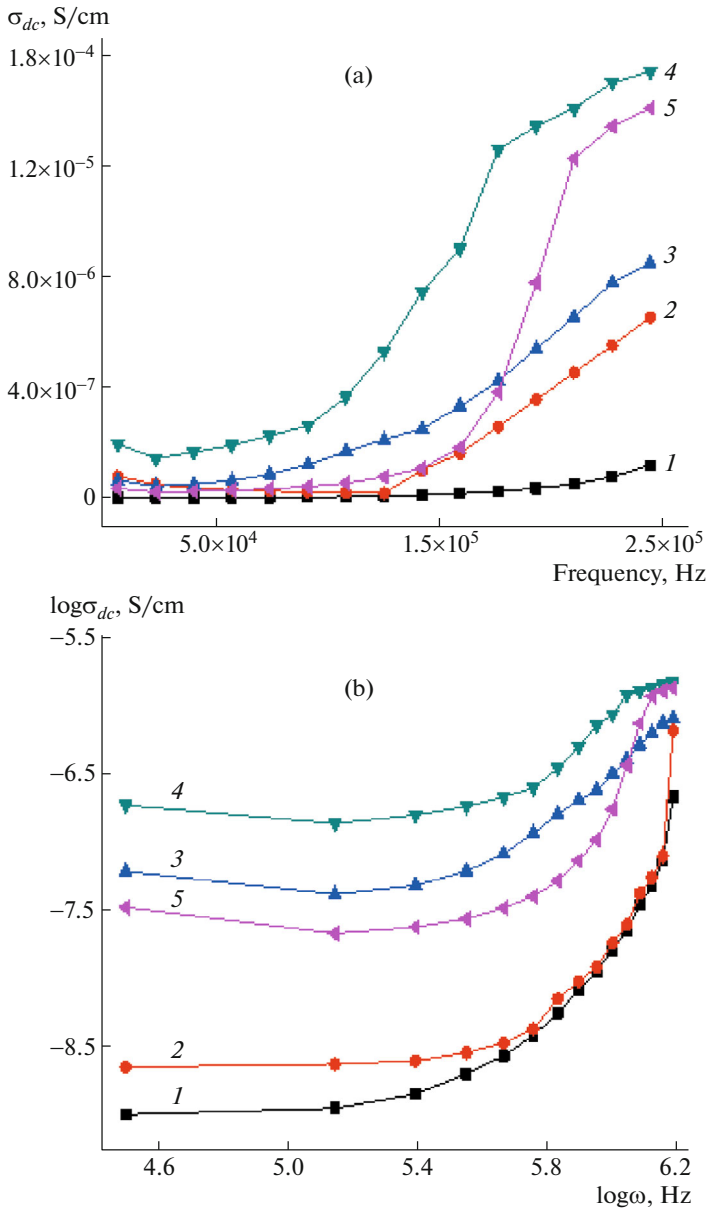

Fig. 7. (Color online) Variation of (a) dc and of (b) log dc conductivity with frequency of polymer electrolyte films for different wt % ratios at 303 K: (*1*) pure PVP, (*2*) (95 : 5), (*3*) (90 : 10), (*4*) (85 : 15), (*5*) (80 : 20).

ization that takes place at the electrode and electrolyte interfaces and the dipolar relaxation process.

The change in imaginary part of dielectric permittivity with frequency of Mg-Al_2O_3 content is shown in Fig. 6b. The value of ε" seems to decrease with increasing frequency at room temperature in nanocomposite polymer electrolyte [39]. Free charge motion takes place at the electrode-electrolyte interface for higher values of imaginary part ε".

The variation of tangent loss δ with log frequency *f* for various wt % ratios of the polymer electrolyte samples is shown in Fig. 6c. The decrease in the tangent loss results with increase in the log frequency; this may be due to the reduced proportion of amorphous material leading to reduction in the magnitude of dispersion. The appearance of peaks suggests the presence of relaxing dipoles in the samples and also with electrical relaxation process or inability of dipoles.

Figure 7 denotes the fact that when the frequency is increased, the ionic conductivity and the oriental source of polarizability increase; this is due to the transfer of mobile ions which causes a constant value of dielectric constant [37]. The plateau region describes the space charge polarization at the blocking electrode and is associated with dc conductivity σ_{dc} of the complexed polymer electrolyte. As shown in

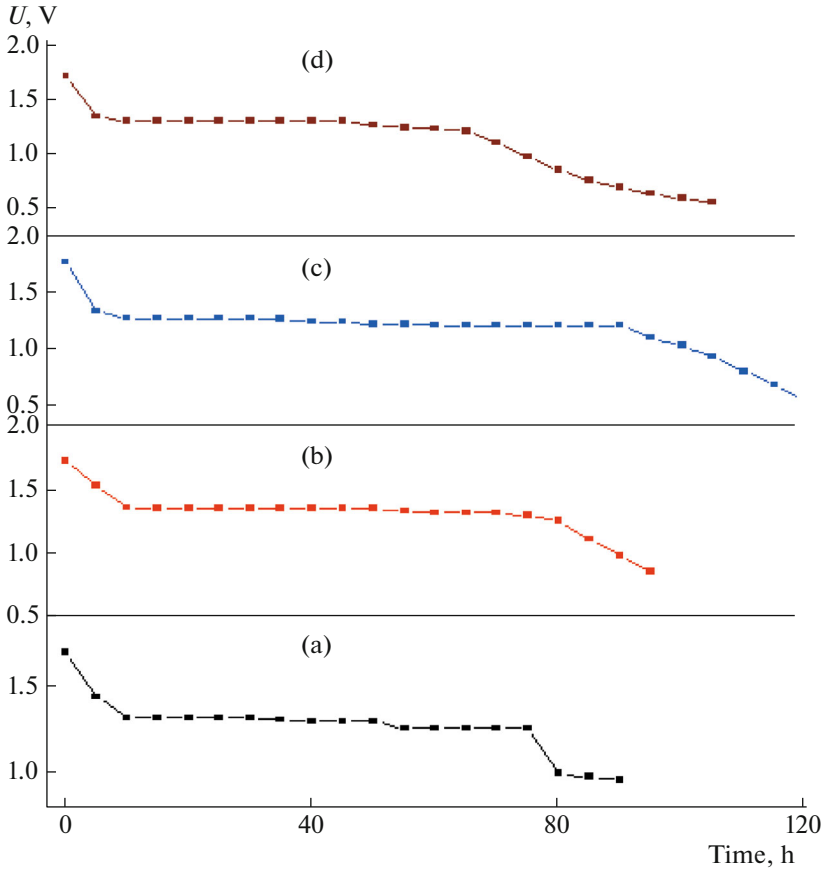

Fig. 8. (Color online) Discharge characteristics of polymer electrolyte films for different wt % ratios of PVP: (a) (95 : 5), (b) (90 : 10), (c) (85 : 15), (d) (80 : 20).

Fig. 7a, the high frequency dispersion region, the ionic conductivity increases with the increase in frequency which is associated with conductivity σ_{dc} of the polymer electrolyte. However at high frequencies the conductivity variation with temperatures is much less than that of lower frequencies. This may be due to large scale heterogeneity of nanoparticles doped in the complex and replacement by small-scale heterogeneity of nanoparticles of Mg-Al_2O_3 [38]. When the nanoparticles content is enhanced in the different wt% ratios the segregation of ions takes place and it reduces the polarizability of polymer electrolyte system.

Variation of dielectric constant ε' with the frequency dependent for both electrolytes is proportional to ωn^{-1}, indicating non-Debye dependence [40]. This indicates the conductivity dependence on the relaxation process, as shown in Fig. 7 band it is a non-exponential in time [41].This interface and existence of space charge polarization, where there is time for the charges to build up at the interface before the applied field changes direction, giving a large value of $\dot{\varepsilon}$ [42]. With the increasing rate of the electric field reversal, there is no time for charge build-up at the interface with increasing frequencies. The polarization due to charge accumulation decreases and it leads to decrease in the value of ε' [43, 44].

Discharge Characteristics

A solid state polymer battery has been fabricated with the configuration of Mg^+ (anode)/polymer electrolyte/(I + C + electrolyte)/(cathode) at room tem-

Table 3. Cell parameter values for different compositions of polymer films PVP + $MgCl_2 \cdot 6H_2O$ + Al_2O_3

Parameters	95 : 05	90 : 10	85 : 15	80 : 20
Cell weight, g	1.98	1.99	1.98	1.98
Area of the cell, cm^2	1.45	1.45	1.45	1.45
Open circuit voltage (OCV)	1.4	1.5	1.7	1.9
Discharge time, h	86	90	120	95
Current density, mA/cm^2	1.7	2.0	1.4	1.8
Discharge cell, mA/h	29.1	17.5	32.2	27.4
Power density, W/kg	1.76	2.18	1.80	2.36
Energy density, W h/kg	152	197	276	298

Table 4. Cell parameters of different solid polymer electrolytes

Solid state electrochemical cell	Open circuit voltage, V	Discharge time, h	Reference
Na/(PVA + NaF)/(I_2 + C + electrolyte)	2.53	112	23
Mg/(PVA+ $Mg(CH_3COO)_2$)/(I_2 + C+ electrolyte)	1.84	87	24
K/(PVP + PVA + $KClO_3$)/(I_2 + C + electrolyte)	2.00	52	25
K/(PVP + PVA + $KBrO_3$)/(I_2 + C + electrolyte)	2.30	72	26
Mg/(PEG + $Mg(CH_3COO)_2$)/(I_2+ C +electrolyte)	1.84	32	27
Ag/(PEO + $AgNO_3$)/(I_2 + C + electrolyte)	0.59	48	28
Na/(PVA + $CH_3COONa_3H_2O$)/(I_2 + C +electrolyte)	1.9	75	29
Mg/[PVP + $MgCl_2 \cdot 6H_2O$ + Al_2O_3]/(I_2 + C + electrolyte)	1.9	120	Present

perature. The anode and cathode materials were made in the form of a pellet with the thickness of 1 mm. In the anode region the charge carrier's takes place due to the magnesium metal and the mixture of iodine and carbon powder is acting as active cathode material which enhances its electronic conductivity [45]. The discharge characteristics were studied for a constant load of 100 kΩ. Current density was calculated using short circuit value and the area of the cell. Power density values were obtained by taking weight of the cell into consideration. Energy density values were calculated by evaluating the time taken for plateau region from Fig. 8. Initially, a rapid decrease in the voltage is occurred; it may be due to the polarization and the formation of thin layer of magnesium salt at the electrode/electrolyte interfaces [46]. Figure 8 shows the discharge characteristics of solid state polymer battery having highest conductivity for 85 : 15 having long durability and exhibits better performance. The cell parameters like open circuit voltage, short circuit current, current density and power density etc. were calculated and mentioned in Table 3 and the other cell parameters are compared in Table 4. From the data, it is clear that the open circuit voltage was found to be greater in PVP + $MgCl_2 \cdot 6H_2O$ + Al_2O_3 (85 : 15) cell comparable to the other complexed films. This may be due to the high ionic conductivity when compared to other systems. While increasing wt % ratios of the salt the open circuit voltage and discharge time of the cell for the polymer electrolyte increases predominantly. From the conductivity studies it is clear that the discharge time is large for 15 wt % salt concentration.

CONCLUSIONS

Solid polymer electrolyte films were prepared by adding Al_2O_3 particles to PVP-$MgCl_2 \cdot 6H_2O$ salt using solution cast technique. The structural analysis of pure PVP complexed with $MgCl_2 \cdot 6H_2O$ salt showed crystalline orthorhombic lattice indicating its semi-crystalline nature. SEM images reveal that the heterogeneous phase of nanocomposite polymer electrolyte systems. From the Optical analysis, it is revealed that the films with the lowest activation energy have the highest ionic conductivity. From the conductivity studies it is evident that the highest conductivity for PVP + $MgCl_2 \cdot 6H_2O$ + Al_2O_3 (85 : 15) was found to be 1.22×10^{-6} S/cm at room temperature. By using these polymer electrolyte films a solid state polymer battery has been fabricated and the discharge characteristics were studied.

ACKNOWLEDGMENTS

The authors are thankful to Dr. K. Satyanarayana, President, Dr. M. Ramamoorthy (Chancellor) and Dr. L. S. S. Reddy (Vice chancellor) of K. L. University for their constant encouragement. The authors specially thank Dr. D. Prema Chandra Sagar (Pro Chancellor Dayananda Sagar University), Prof. A.N.N. Murthy (Vice Chancellor, DSU) and Dr. B.R. Lakshmikantha, Principal, Dayananda Sagar Academy of Technology and Management, Bangalore for their kind support and motivation. The authors also thank faculty members of Department of Physics K.L. University, for their cooperation in completion of this work.

REFERENCES

1. M. Jaipal Reddy, J. Siva Kumar, U. V. Subba Rao, and P. P. Chu, Solid State Ionics **177**, 253 (2006)
2. K. Naresh Kumar, T. Sreekanth, M. Jaipal Reddy, and U. V. Subba Rao, J. Power Sources **101**, 130 (2001).
3. K. Murata, Electrochem. Acta **40**, 2177 (1995).
4. X. F. Yang, G. C. Wang, R. Y. Wang, and X. W. Li, Electrochim. Acta **55**, 5414 (2010).
5. R. A. Irgashev, A. A. Karmatsky, S. A. Kozyukhin, V. K. Ivanov, A. Sadovnikov, V. V. Kozik, V. A. Grinberg, V. V. Emets, G. L. Rusinov, and V. N. Charushin, Synth. Met. **199**, 152 (2015).
6. D. E. Fenton, J. M. Parker, and P. V. Wright, Polymer **14**, 589 (1973).
7. P. V. Wright, Brit. Polym. J. **7**, 319 (1975).

8. M. S. Whittingham, W. Wippner, and H. Schulz, Solid State Ionics **28**, 1 (1988).
9. M. B. Armand, Solid State Ionics **9**–**10**, 745 (1983).
10. S. Li, M. M. Lin, M. S. Toprak, D. K. Kim, and M. Muhammed, Nano Rev. **1**, 5214 (2010).
11. K. I. Winey and R. A. Vaia, MRS Bull. **32**, 314 (2007).
12. C. P. Collier, R. J. Saykally, J. J. Shiang, S. E. Henrichs, and J. R. Heath, Science **277**, 1978 (1997).
13. W. A. Lopes and H. M. Jaeger, Nature **414**, 735 (2001).
14. T. A. Taton, C. A. Mirkin, and R. L. Letsinger, Science **289**, 1757 (2000).
15. M. Forsyth, D. R. Mac Farlene, A. Best, J. Adebahr, P. Jacobsson, and A. J. Hill, Solid State Ionics **147**, 203 (2002).
16. Y.-Y. Yu, W.-C. Chien, and T.-W. Tsai, Polym. Test. **29**, 33 (2010).
17. J. Xi, X. Qiu, S. Zheng, and X. Tang, Polymer **46**, 5702 (2005).
18. *The Primary Battery*, Ed. by N. C. Cahoon and G. W. Heise (J. Wiley and Sons, New York, 1976), p. 149.
19. T. D. Gregory, R. J. Hoffmann, ans R. C. Winterton, J. Electrochem. Soc. **137**, 775 (1990).
20. E. M. Abdelrazeka, H. M. Ragabb, and. M. Abdelaziza, Plast.-Polym. Technol. Sci. **2**, 1 (2013).
21. J. E. Weston and B.C.H. Steele, Solid State Ionics **7**, 75 (1982).
22. J. Cho and M. Liu, Electrochim. Acta **42**, 1481 (1997).
23. X. Cheng, K. W. Putz, C. D. Wood, and L. C. Brinson, Macromol. Rapid Commun. **36**, 391 (2015).
24. T. Lan and J. M. Torkelson, Polymer **55**, 1249 (2014).
25. J. Choi, M. J. A. Hore, N. Clarke, K. I. Winey, and R. J. Composto, Macromolecules **47**, 2404 (2014)
26. H. Althues, J. Henle, and S. Kaskel, Chem. Soc. Rev. **36**, 1454 (2007).
27. R. M. Hodge, G. H. Edward, and G. P. Simon, Polymer **37**, 1371 (1996).
28. S. A. M. Noor, A. Ahmad, I. A. Talib, and M. Y. A. Rehman, Ionics **16**, 161 (2010).
29. D. S. Davis and T. S. Shalliday, Phys. Rev. **1020**, 118 (1960).
30. R. M. Khafagy, J. Alloys Compd. **509**, 9849 (2011).
31. J. Arias-Pardilla, H. J. Salavagione, C. Barbero, E. Morallón, and J. L. Vázquez, Eur. Polym. J. **42**, 1521 (2006).
32. D. K. Pradhan, R. N. P. Choudhary, and B. K. Samantaray, Int. J. Electrochem. Sci. **3**, 597 (2008).
33. P. W. Davis and T. S. Shilliday, Phys. Rev. **118**, 1020 (1960).
34. G. K. M. Thutupalli and S. G. Tomlin, J. Phys. D: Appl. Phys. **9**, 1639 (1976).
35. C. Venkata Subba Rao, M. Ravi, V. Raja, P. Balji Bhargav, A. K. Sharma, and V. V. R. Narasimha Rao, Iran Polym. J. **21**, 531 (2012).
36. M. Abdelaziz and M. M. Ghannam, Phys. B (Amsterdam, Neth.) **405**, 958 (2010).
37. R. Bhaskaran, S. Selvasekarapandian, N. Kuwata, J. Kawamura, and T. Hattori, Mater. Chem. Phys. **98**, 5 (2006).
38. K. Pandey, M. M. Wivedi, I. M. L. Das, and M. A. Singh, J. Electroceram. **25**, 99 (2010).
39. G. Gondivaraj, N. Baskaran, K. Shahi, and P. Monoravi, Solid State Ionics **76**, 47 (1995).
40. P. Balaya and P. S. Goyal, J. Non.-Cryst. Solids **351**, 1573 (2005).
41. S. R. Majid and A. K. Arof, Phys. B (Amsterdam, Neth.) **390**, 215 (2007).
42. A. Molak, E. Ksepko, I. Gruszka,A. Ratuszna, M. Paluch, and Z. Ujma, Solid State Ionics **176**, 1439 (2005).
43. E. El Shafee, Carbohydr. Polym. **31**, 93 (1996).
44. A. R. Polu and R. Kumar, Int. J. Polym. Mater. **62**, 76 (2012).
45. J. Ravi, M. Pavani, Y. Kumar, K. K. Bhvani, A. K. Sharma, and V. V. R. N. Rao, Mater. Chem. Phys. **130**, 442 (2011).
46. S. K. Shahenoor Basha, G. Sunita Sundari, and K. Vijay Kumar, Int. J. Chem. Technol. **9**, 165 (2016).